Available online at www.sciencedirect.com
SCIENCE DIRECT®
Journal of Solid State Chemistry 178 (2005) 3130–3136
JOURNAL OF SOLID STATE CHEMISTRY
www.elsevier.com/locate/jssc

# Controlled morphology synthesis of β-FeOOH and the phase transition to $Fe_2O_3$

Hua-Feng Shao, Xue-Feng Qian*, Jie Yin, Zi-Kang Zhu

*School of Chemistry and Chemical Technology, State Key Laboratory of Composite Materials, Shanghai Jiao Tong University, Shanghai 200240, PR China*

Received 2 June 2005; received in revised form 9 July 2005; accepted 17 July 2005
Available online 24 August 2005

**Abstract**

The hexagram and arrayed β-FeOOH nanorods were first synthesized free of surfactants through the solvent-thermal method. X-ray powder diffraction (XRD), transmission electron microscopy (TEM), selected area electron diffraction (SAED), field emission scanning electron microscopy (FESEM), energy dispersive X-ray spectrum (EDAX) and thermal gravimetric analysis (TGA) were used to characterize the as-prepared products. The TEM and FESEM images showed that hexagram β-FeOOH and arrayed rod-like β-FeOOH with an average diameter of 10–15 nm and an average length of 100 nm (aspect ratio is about 10) were prepared. Electrochemical tests show that these nanorods deliver a large discharge capacity of 277 mA h $g^{-1}$ versus Li metal at 0.1 mA $cm^{-2}$ (voltage at 1.5–4.2 V). Treated the as-synthesized rod-like β-FeOOH by annealing, rhombus hematite was obtained.


*Keywords:* β-FeOOH; Nanorod; Solvent-thermal; $Fe_2O_3$; Electrochemical

## 1. Introduction

Due to the importance of the shape and texture of materials in determining their macroscopical properties [1–3], how to control the morphologies of micro- and nanoscale materials has become an important goal of modern materials chemistry. Up to now, many developments have been made and many novel morphologies such as nanoribbon [4], nannocube, nanofiber, dendrite- and star-like nanostructures [5] have been synthesized successfully.

It is well known that iron compounds are abundant in nature, and hydroxides (FeOOH) and oxides ($Fe_2O_3$) have been extensively used in the production of pigments, catalysts, gas sensors, magnetic recording media and raw materials of hard and soft magnets [6–10]. With similar structures, such as α-, β-, γ-type, iron oxyhydroxides have distinctive properties and have been widely used as electrode materials and precursors in lithium batteries [11–13]. Among the iron compounds, the iron oxyhydroxide phase akaganeite, β-type FeOOH, has a large tunnel-type structure where iron atoms are strongly bonded to the framework [12], and lithium can be intercalated and extracted freely in the tunnels (2 × 2) during discharge and charge processes. Furthermore, as a promising candidate for an electrode material, β-FeOOH exhibits good electrochemical performance with a high theoretical discharge capacity (283 mA h $g^{-1}$). Moreover, β-FeOOH is a semiconductor with a band gap of 2.12 eV [14] and can also be used in oxidation/reduction reactions and hydroprocessing of coal as catalysts [15], and in the preparation of ferromagnetic materials, such as γ-$Fe_2O_3$ [16]. Thus, oriented alignment of β-FeOOH nanowires/nanorods might have potential applications in lithium batteries, semiconductor electronics, and the preparation of magnetic recording media materials.

*Corresponding author. Fax: +86 21 54741297.
*E-mail address:* xfqian@sjtu.edu.cn (X.-F. Qian).

0022-4596/$ - see front matter © 2005 Elsevier Inc. All rights reserved.
doi:10.1016/j.jssc.2005.07.011

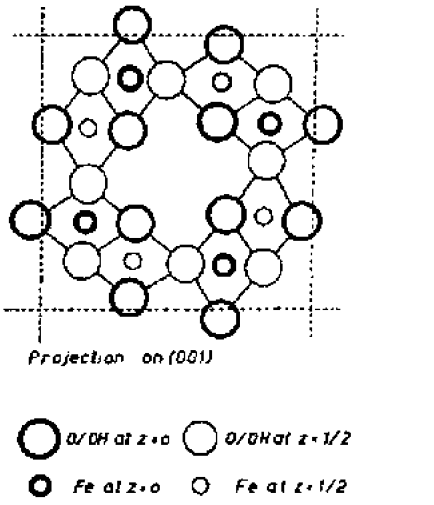

The Sketch of the β-FeOOH framework

For many years, one-dimensional (1D) nanostructure systems have attracted increasing interest for their crucial role in future technological advances in electronics, optoelectronics and memory devices [17–19]. And the 1D structure has been considered as the smallest dimension structures to study the theory of nanostructure properties. Recent researches on nanowires and nanorods are expanding rapidly into their assembly to two- (2D) and three-dimensional (3D) ordered superstructures [16]. However, to the best of our knowledge, the surfactant-free and one-step solvent-thermal synthesis of 1D single-crystal $\beta$-FeOOH nanorod arrays have not been reported, and the synthesis of 1D nanostructure $\beta$-FeOOH may provide the possibility to detect the theoretical operating limits of lithium batteries. Herein we report the synthesis of $\beta$-FeOOH nanorods via a simple one-step solvent-thermal method and the electrochemical properties for possible use as an electrode material in lithium ion batteries. The rhombus hematite was synthesized by annealing the rod-like $\beta$-FeOOH.

## 2. Experimental section

### 2.1. Experimental

Analytically pure $FeCl_3 \cdot 6H_2O$, $NaNO_3$ and HCl (concentrated) (Shanghai Chemical Reagent Co., Ltd) were used as reactants without further purification. In a typical process, a certain amount of $FeCl_3 \cdot 6H_2O$ and $NaNO_3$ was dissolved in distilled water or water/ethanol co-solvent with magnetic stirring, and HCl was used to adjust the pH value. Then the above solution was transferred into a Teflon-lined stainless steel autoclave. The sealed autoclave was maintained at 120 °C for 2 h, and then cooled to room temperature naturally. The resulting product was collected by ultraspeed centrifugation and washed several times with absolute ethanol and distilled water, then vacuum dried at 60 °C for 6 h. The detail experimental conditions, the phase composition and morphologies of sample are listed in Table 1. The as-synthesized sample was calcined at 550 °C in muffle at air to obtain $Fe_2O_3$.

### 2.2. Characterization

The powder X-ray diffraction (XRD) patterns were recorded at a scanning rate of $4^\circ\,min^{-1}$ in the $2\theta$ range of 10–70° using a Shimadzu XRD-6000 X-ray diffractometer with Cu-$K\alpha$ radiation ($\lambda = 1.5406$ Å). The morphologies and micro-/nanostructures of the as-synthesized product were further observed using a JEOL JEM-100CXII transmission electron microscope at the acceleration voltage 100 KV. The samples were prepared by mounting a drop of the resulting aqueous solution on carbon-coated Cu grids and were allowed to dry in air. Selected area electron diffraction (SAED) was also recorded on the JEOL TEM. Sirion 200 field emission scanning electron microscopy (FESEM) with an acceleration voltage 10 kV was used to observe the

Table 1
The detailed experimental conditions, the phase composition and morphologies of sample

| Sample | [$FeCl_3$] (M) | [HCl] (M) | [$NaNO_3$] (M) | Time (h) | Phase composition as found by XRD | Solvent ($C_2H_5OH$/$H_2O$) (v/v) | Morphology determined by TEM |
|---|---|---|---|---|---|---|---|
| I | 0.15 | — | — | 2 | $\beta$-FeOOH | 5:15 | Arrayed nanorod |
| II | 0.15 | 0.09 | 1 | 2 | $\beta$-FeOOH | 5:15 | Hexagram |
| III | 0.15 | 0.09 | 1 | 2 | $\beta$-FeOOH | 0:20 | Rod |
| IV | 0.15 | 0.09 | 1 | 2 | $\beta$-FeOOH | 15:5 | Bundle of fibers |
| V | 0.15 | 0.09 | 1 | 2 | $\beta$-FeOOH | 20:0 | Bundle of fibers |
| VI | 0.15 | — | 1 | 2 | $\beta$-FeOOH | 0:20 | Accumulation of nanorods |
| VII | 0.15 | — | 1 | 2 | $\beta$-FeOOH | 5:15 | Rod |
| VIII | 0.15 | — | 1 | 2 | $\beta$-FeOOH | 10:10 | Rod |
| IX | 0.15 | — | 1 | 2 | $\beta$-FeOOH | 15:5 | Rod |
| X | 0.15 | — | — | 2 | — | 10:10 | — |

Reaction temperature: 120 °C.

morphologies of the as-synthesized product. Energy dispersive X-ray spectrum (EDAX FALCON), linked with JSM-6360VL scanning electron microscope, was used to analyze the element distributions. TGA analysis was performed on a PE Instruments TGA-7. A total of 10–12 mg samples were heated from room temperature to 600 °C at a rate of 20 °C $min^{-1}$ under nitrogen. The pH value was measured by the pHs-25 numeric pH meter (Shanghai RiDao Scientific Instrument Ltd. Co.). Electrochemical tests were conducted with a button battery. The positive electrodes were fabricated by pasting slurries of the as-synthesized sample (80 wt%), Super P (10 wt%) and polyvinylidene (PVDF, 10 wt%) dissolved in *N*-methylpyrrolidinone (NMP) on Al foil strip. Then the strip was dried at 100 °C for 12 h in oven, and pressed and kept at 100 °C for 5 h in a vacuum. Metallic lithium was used as the anode. The electrolyte was 1 M $LiPF_6$ in a 1:1 mixture of ethylene carbonate (EC)/diethyl carbonate (DEC). The cells were assembled in a glove box filled with highly pure argon gas ($O_2$ and $H_2O$ levels less than 5 ppm). The cells were cycled in 1.5–4.2 V at a current density of 0.1 mA $cm^{-2}$.

## 3. Results and discussion

Fig. 1 shows the XRD patterns of the as-synthesized sample. Pattern I shows that the XRD pattern of the sample I matched the diffraction of monoclinic akaganeite (JCPDS card No. 42-1315) very well with cell constants of (a) 10.60 Å, (b) 3.04 Å and (c) 10.51 Å, and no impurity peak can be detected. The EDAX analysis (Fig. 2) indicated that the as-synthesized akaganeite contained three elements: Fe, O and Cl, and no H element was found due to the resolution of the EDAX. According to the report of Richmond et al. [20], chloride

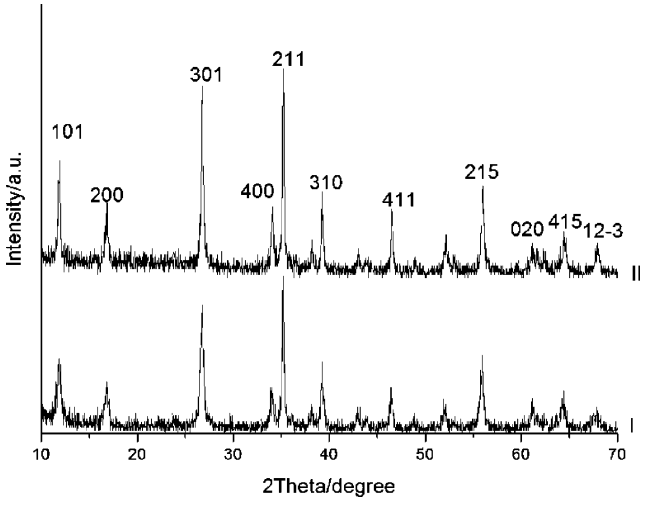


Fig. 1. The XRD patterns of the as-synthesized β-FeOOH (I) nanorod; (II) hexagram.

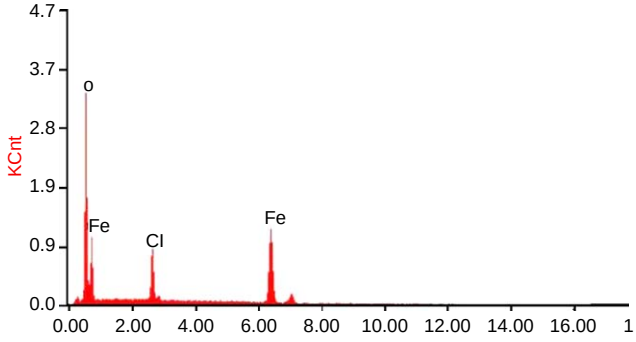


Fig. 2. The EDAX analysis of the as-synthesized sample.

anions, partly substituting for hydroxide, are believed to play an important role in stabilizing the tunnel structure of the akaganeite (β-FeOOH). Combining with the result of XRD analysis, we speculate that the as-synthesized compounds still have the H element. According to the structure formula $FeO(OH)_{1-x}Cl_x$ [20], it can be easily deduced that the ratio of O:Cl equals to $(2-x):x$. Then from the results of the EDAX, which showed the atom ratio of O:Cl is 58.63:6.89, we can deduce $x = 0.21$ by the simple calculation. Similarly, the factor $x$ of the chloride element was 0.2 through the content of Fe and Cl from the EDAX. The molecular structure of the as-prepared β-FeOOH can be expressed as $FeO(OH)_{0.79}Cl_{0.21}$.

Fig. 3 is the TEM images of as-synthesized sample that was prepared in the mixed solvent of ethanol and distilled water (ratio of ethanol to water equals 5:15). Fig. 3a shows the nanorods are arranged compactly and tidily on the copper grid. The average length of the nanorod is about 150 nm. In Fig 3b some uniform spheres with a diameter about 10–15 nm are presented in the photograph besides the nanorod array, and these spheres are regularly arranged (Figs. 3b and c). From the FESEM image (Fig. 4) we can find that all the obtained materials are rod-like, and most of the nanorods are closely assembled. Combining the photographs of TEM and FESEM, it can be easily deduced that the presented dots in TEM are the top view of the arrayed nanorods. From the analysis above, we deduced that the dots in Figs. 3b and c were not particles but the top view of the arrayed nanorods due to the random orientation of the nanorod arrays on the TEM grid. The SAED pattern (Fig. 3d) reveals that single-crystalline β-FeOOH nanorods are obtained. Recently, some researches have focused on the self-assembly of nanocrystals to form the 2D or 3D super-lattice structures. For example, Dumestre et al. [21] studied the super-lattice self-assembly of the cobalt nanorods and presumed that the formation of regular nanorods may result from the initial inclusion of the monodisperse spherical particles into the 3D super-lattices. Hideatsu Maeda et al. [22]

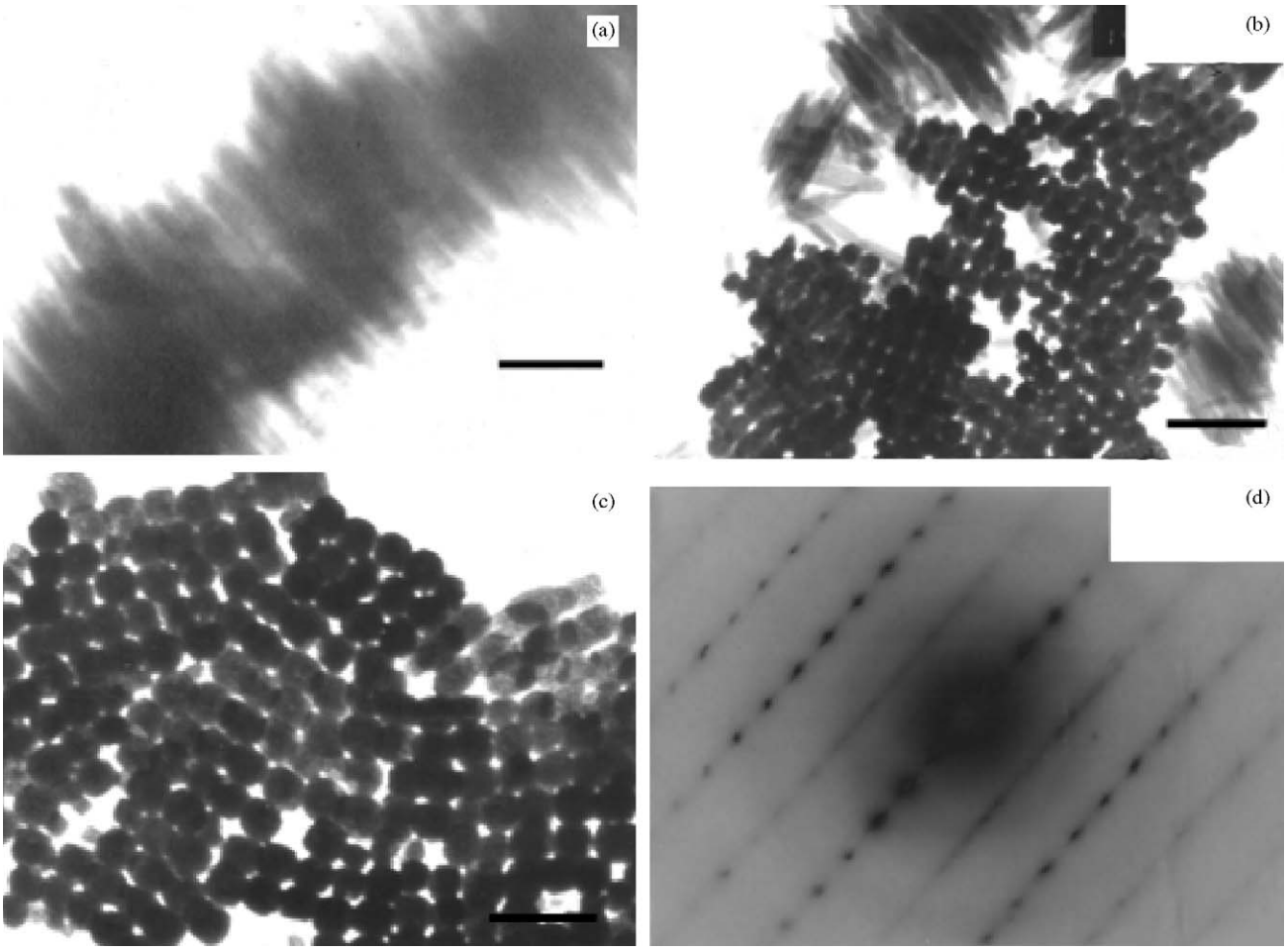


Fig. 3. The TEM images of the as-synthesized sample I. Scale bar: (a, b) 50 nm; (c) 40 nm.

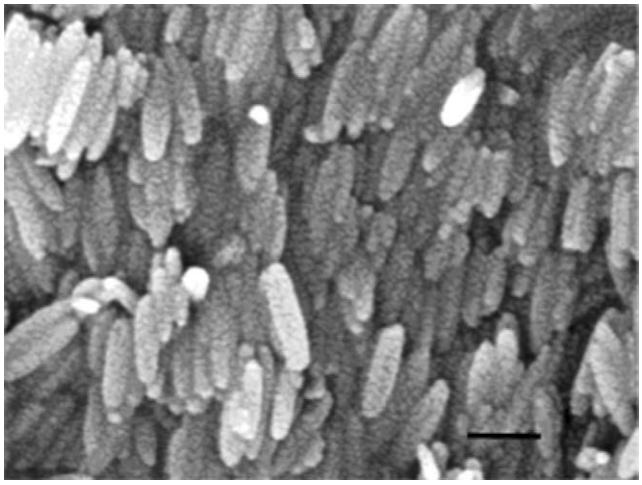

Fig. 4. The FESEM image of the as-synthesized product. Scale bar: 50 nm.

studied the $\beta$-FeOOH smectic layer which formed due to the dragging force coming from the surface tensions acting on the droplet edge line during the evaporation process used Atomic Force Microscopy (AFM). From the FESEM image (Fig. 4), the as-fabricated $\beta$-FeOOH was also assembled to a relatively tight array. There was no evaporation of solvent during the preparation process of the FESEM, so the as-synthesized $\beta$-FeOOH nanorods self-assemble to a relatively tight array due to the dipolar effect during the growth process but not the evaporation process of the solvent during the preparation process of the TEM sample.

At the same time, the ratio of $C_2H_5OH$ and $H_2O$ also has great effects on the morphologies of the obtained materials. Thicker rod-like nano-$\beta$-FeOOH can be obtained by modifying the ratio of the solvent (see Table 1).

As is well known, $OH^-$ can form a bridge between two iron ions in acid solution containing $Fe^{3+}$. Handa et al. suggested that $[(HO)_xCl_yFeO_2FeCl_y(OH)_x]_6$. $(x+y=4)$ can be formed in the solution of $FeCl_3$ [23]. From the pH value of $FeCl_3$ solutions (Table 2), the pH value decreased from 1.68 to 0.55 with the increase of the ratio of ethanol in the solution. So the function of ethanol is to slow the hydrolysis of $Fe^{3+}$ by

Table 2
The effect of ratio of ethanol to water on pH value

| Sample | Ratio of ethanol to water (v/v) | pH value |
|---|---|---|
| 1 | 0:20 | 1.68 |
| 2 | 5:15 | 1.55 |
| 3 | 10:10 | 1.35 |
| 4 | 15:5 | 1.32 |
| 5 | 20:0 | 0.55 |

No $NaNO_3$ and HCl in the solutions.

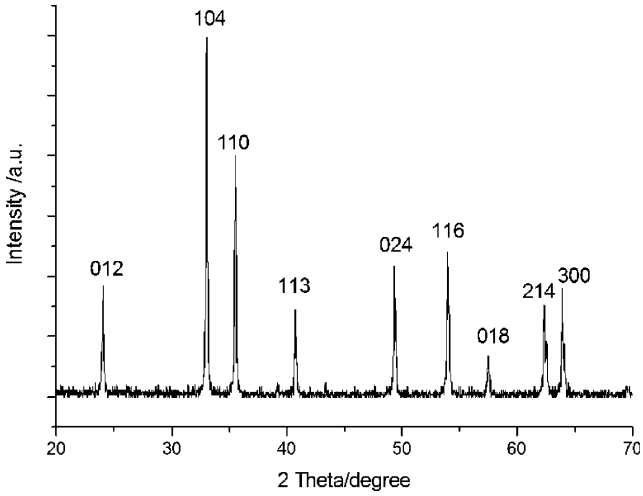


Fig. 5. The XRD pattern after annealing the as-synthesized sample I.

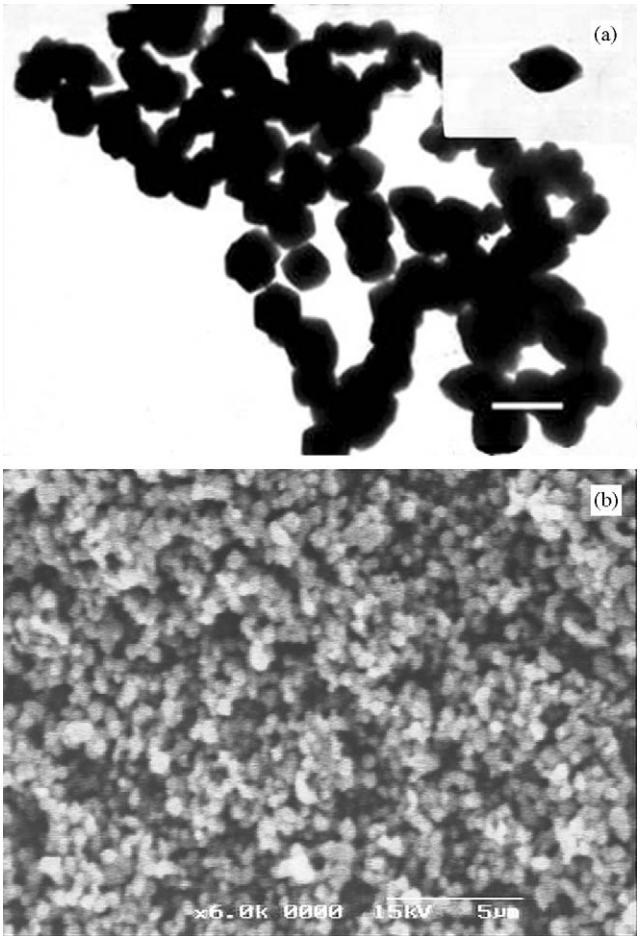


Fig. 6. The morphology of the obtained hematite. Scale bar in TEM image: 500 nm.

decreasing the pH value. On the other hand, ethanol as a solvent in the solvent-thermal process can reach a critical state [24], and then modify the physico-chemical properties of the reactant which also affects the formation and morphology of the crystal during the heating process.

From the TGA curve (Fig. S1) of the as-synthesized sample, it can be seen that $\beta$-FeOOH had a weight loss at 42–195 °C due to the loss of $H_2O$, and a second weight loss at 195–550 °C due to the phase transformation of $\beta$-FeOOH to hematite. Fig. 5 is the XRD pattern of $\beta$-FeOOH after being calcined at 550 °C. In the obtained XRD pattern, all the diffraction peaks can be indexed to the hematite (JCPDS card No. 33-664). It indicated that the $\beta$-FeOOH has been transferred into the hematite phase after being calcined. Fig. 6 shows the TEM and SEM images of the as-synthesized hematite. The rod-like $\beta$-FeOOH has transferred to rhombus hematite after being calcined.

In the experiment, a certain concentration of $NaNO_3$ and HCl has important effects on the morphologies of the obtained $\beta$-FeOOH. Vayssieres [25] pointed out that the additional $NaNO_3$ can increase the ionic strength and further decrease the interfacial tension of the system, and it is favorable to form $\beta$-FeOOH rather than hematite ($Fe_2O_3$) which is apt to form in the Fe–O phase diagram for most temperatures and pressures. In our experiment, all the products are $\beta$-FeOOH (Table 1) whether $NaNO_3$ was added or not. This phenomenon is due to the use of ethanol as the co-solvent, which differs from the work of Vayssieres (with distilled water as solvent). It is well known that the surface tension of distilled water is up to $73 \times 10^{-3}$ N m$^{-1}$ and ethanol is only $23 \times 10^{-3}$ at 20 °C. So the interfacial tension of the ethanol/water system is low enough to form $\beta$-FeOOH without the presence of $NaNO_3$. From the TEM image (Fig. 7), hexagram $\beta$-FeOOH was obtained when $NaNO_3$ was added with same ratio of ethanol and water (sample II). Figs. 7a and b show that the obtained $\beta$-FeOOH is in hexagram morphology, and the diameter of the joint is about 50 nm, the end of the nanorod is not sharp. In Fig. 7b, some single horn existed besides the hexagram $\beta$-FeOOH, it indicated that the hexagram $\beta$-FeOOH was formed through six separate horns. The XRD patterns (curve 2 in Fig. 1) also can be indexed to the akaganeite (JCPDS card No. 42-1315).

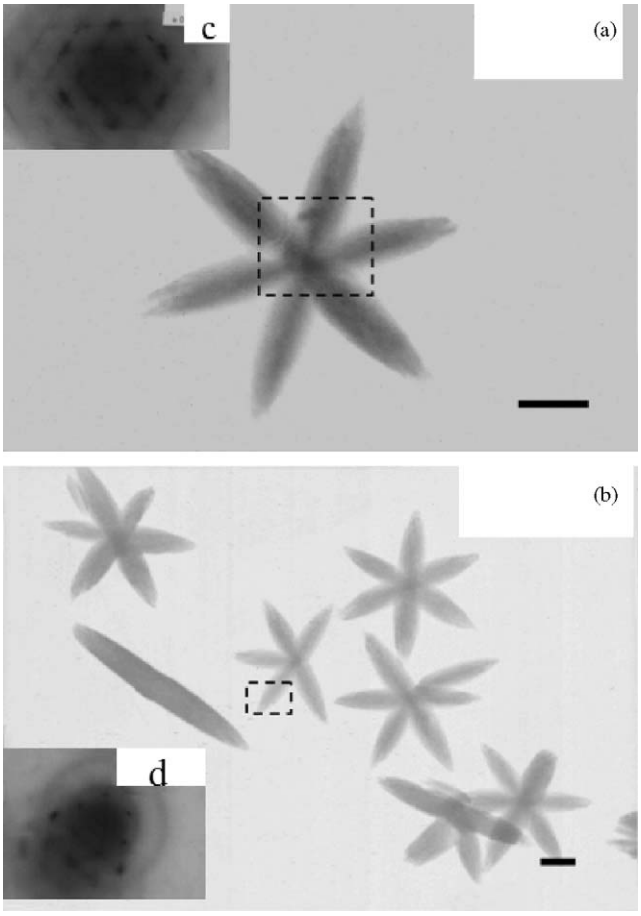


Fig. 7. The TEM images of the as-synthesized sample II. Inset (c) and (d) is the SAED of the selected area (the dashed rectangle). Scale bar in all images: 100 nm.

In the experiment process, we find that the pH value also has many effects on the morphologies of $\beta$-FeOOH. It is well known that the $Fe^{3+}$ is easy to hydrolyse in solution and form Fe $(OH)_3$, so the low pH value of the system is beneficial to form $\beta$-FeOOH rather than Fe $(OH)_3$ [25]. According to the discussion above, introducing ethanol as co-solvent can decrease the pH value of the system obviously. So whether is HCl added or not, all the obtained products are $\beta$-FeOOH. On the other hand, single rod-like $\beta$-FeOOH with thicker diameters ($>15$ nm) was obtained (Table 1, samples VII, VIII and IX; Fig. S2a) without adding HCl, while only bundles of fiber (with diameter about several nanometers, Fig. S2b) were obtained in the presence of HCl (Table 1, samples IV and V). The mechanism of the formation of this morphology might be described as follows:

(1) Nucleation stage. Under a certain temperature and pressure, the $Fe^{3+}$ ions changed to $\beta$-FeOOH rapidly.
(2) The stage of growth. The $\beta$-FeOOH nanorods formed in the solution.

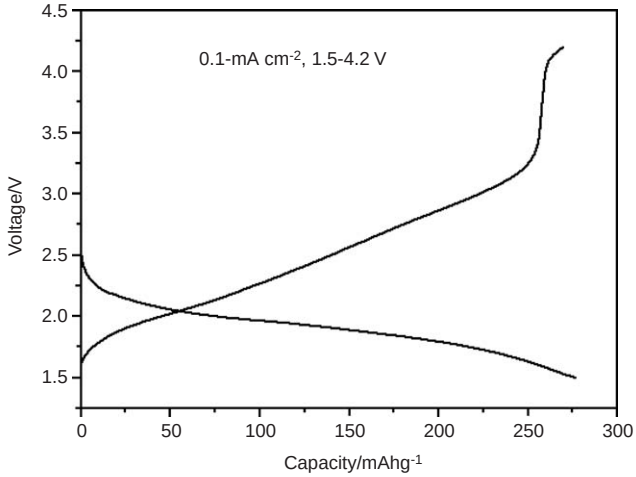


Fig. 8.

(3) Linkage stage. The as-formed nanorods linked to form a single-crystalline hexagram.

Electrochemical performances of the as-synthesized FeOOH in the cell configuration $\beta$-FeOOH/Li have been tested. Fig. 8 shows the voltage versus capacity for the cell between 1.5 and 4.2 V at a current density of 0.1 mA $cm^{-2}$. The reversible capacity of the arrayed $\beta$-FeOOH nanorods in the lithiation–delithiation cycles is around 277 mA h $g^{-1}$, which is very close to the theoretical value (283 mA h $g^{-1}$) [12] and higher than that of $\beta$-FeOOH prepared by the literature (275 mA h $g^{-1}$) [26]. Li ions can be freely intercalated and deintercalated in the $\beta$-FeOOH tunnels during the discharge and charge processes with a high coulombic efficiency for the first cycle up to 97%, and excellent electrochemical properties can be obtained.

## 4. Conclusion

Hexagram and arrayed self-assembly $\beta$-FeOOH nanorods were first synthesized free of surfactant through the solvent-thermal method. With the modification of reaction conditions, $\beta$-FeOOH with different morphologies was obtained. The arrayed $\beta$-FeOOH nanorods have an average diameter of 10–15 nm and an average length of 100 nm (aspect ratio is about 10). Hexagram $\beta$-FeOOH monocrystals with a joint part about 50 nm were also observed. The six horns were not very sharp with slight divarication. The reversible discharge-specific capacity can reach 277 mA h $g^{-1}$ with a high coulombic efficiency for the first cycle up to 97%.

With further annealing treatment of the as-synthesized $\beta$-FeOOH nanorods, rhombus hematite was obtained.

## Acknowledgments

This work was financially supported by the National Natural Foundation of China (50103006), the Shanghai ShuGuang Project (01-SG-15) and the Shanghai Nanomaterials Project (0212nm106).

## Appendix A. Supplementary data

Supplementary data associated with this article can be found in the online version at doi:10.1016/j.jssc.2005.07.011

## References

[1] S. Mann, Angew. Chem. Int. Ed. 39 (2000) 3392.
[2] L.-M. Qi, H. Cölfen, M. Antonietti, Angew. Chem. Int. Ed. 39 (2000) 604.
[3] (a) H. Shi, L. Qi, J. Ma, H. Cheng, J. Am. Chem. Soc. 125 (2003) 3450;
(b) J.-Y. Lao, J.-G. Wen, Z.-F. Ren, Nano Lett. 2 (2002) 1287.
[4] C.-L. Zhu, C.-N. Chen, L.-Y. Hao, Z.-Y. Chen, J. Cryst. Growth 263 (2004) 473.
[5] (a) D.-B. Kuang, A.-W. Xu, Y.-P. Fang, H.-Q. Liu, C. Frommen, D. Fenske, Adv. Mater. 15 (2003) 1747;
(b) Y.-R. Ma, L.-M. Qi, J.-M. Ma, H.-M. Cheng, Cryst. Growth Design 4 (2004) 351.
[6] C. Gong, D. Chen, X. Jiao, Q. Wang, J. Mater. Chem. 12 (2002) 1844.
[7] E. Matijevic, P. Scheiner, J. Colloid Interface Sci. 63 (1978) 509.
[8] M.P. Morales, T. González-Carreenö, C.J. Serna, J. Mater. Res. 7 (1992) 2538.
[9] B. Faust, M. Hoffmann, D. Bachnemann, J. Phys. Chem. 93 (1989) 6371.
[10] G. Neri, A. Bonavita, S. Galvagno, P. Siciliano, S. Capone, Sensor Actuator. B: Chem. 82 (2002) 40.
[11] R. Kanno, T. Shirane, Y. Kawamoto, Y. Takeda, M. Takano, M. Ohashi, Y. Yamaguchi, J. Electrochem. Soc. 143 (1996) 2435.
[12] K. Amine, H. Yasuda, M. Yamachi, J. Power Sources 81–82 (1999) 221.
[13] C.M. Flynn, Chem. Rev. 84 (1984) 31.
[14] A.F. White, Rev. Mineral. 23 (1990) 467.
[15] R.M. Cornell, The Iron Oxides, VCH, New York, 1996.
[16] Y.-J. Xiong, Y. Xie, S.-W. Chen, Z.-Q. Li, Chem. Eur. J. 9 (2003) 4991.
[17] Y. Cui, C.M. Lieber, Science 291 (2001) 851.
[18] X. Wang, X. Chen, L. Gao, H. Zheng, M. Ji, T. Shen, Z. Zhang, J. Cryst. Growth 256 (2003) 123.
[19] X. Wang, Y.-D. Li, J. Am. Chem. Soc. 124 (2002) 2880.
[20] W.R. Richmond, J.G. Hockridge, M. Loan, G.M. Parkinson, Chem. Mater. 16 (2004) 3203.
[21] F. Dumestre, B. Chaudret, C. Amiens, M. Respaud, P. Fejes, P. Renaud, P. Zurcher, Angew. Chem. Int. Ed. 42 (2003) 5213.
[22] Hideatsu Maeda, Yoshiko Maeda, Nano Lett. 2 (2002) 1073.
[23] A. Handa, J. Kobayashi, Y. Ujihira, Appl. Surf. Sci. 20 (1985) 581.
[24] E. Verdon, M. Devalette, G. Demazeau, Mater. Lett. 25 (1995) 127.
[25] L. Vayssieres, N. Beermann, S. Lindquist, A. Hagfeldt, Chem. Mater 13 (2001) 233.
[26] X. Wang, X.-Y. Chen, L.-S. Gao, H.-G. Zheng, M.-R. Ji, C.-M. Tang, T. Shen, Z.-D. Zhang, J. Mater. Chem. 14 (2004) 905.